MedChemComm

RSC Publishing

CONCISE ARTICLE

View Article Online
View Journal | View Issue

Mapping histamine H_4 receptor–ligand binding modes†

Cite this: *Med. Chem. Commun.*, 2013, **4**, 193

Sabine Schultes,‡[ab] Saskia Nijmeijer,‡[a] Harald Engelhardt,[ab] Albert J. Kooistra,[a] Henry F. Vischer,[a] Iwan J. P. de Esch,[a] Eric E. J. Haaksma,[ab] Rob Leurs[a] and Chris de Graaf*[a]

Received 26th July 2012
Accepted 4th September 2012

DOI: 10.1039/c2md20212c

www.rsc.org/medchemcomm

The increasing number of G protein-coupled receptor (GPCR) crystal structures offers new opportunities for histamine receptor homology modeling. However, computational prediction of ligand binding modes in GPCRs such as the histamine H_4 receptor (H_4R), a receptor that plays an important role in inflammation, remains a challenging task. In the current work we have combined complementary *in silico* receptor modeling approaches with *in vitro* ligand structure–activity relationship (SAR) and protein site-directed mutagenesis studies to elucidate the binding modes of different ligand classes in H_4R. By systematically considering different H_4R modelling templates, ligand binding poses, and ligand protonation states in combination with docking and MD simulations we are able to explain ligand-specific mutation effects and subtle differences in ligand SAR. Our studies confirm that a combined theoretical and experimental approach represents a powerful strategy to map ligand–protein interactions.

Introduction

Rational drug design requires detailed knowledge and understanding of the molecular interactions between ligands and proteins. Both ligand- and protein-based *in silico* modeling approaches have been successfully applied to rationalize structure–activity relationships (SAR) and receptor site-directed mutagenesis studies, for the histamine H_4 receptor (H_4R),[1–7] a G protein-coupled receptor (GPCR) that plays an important role in inflammation.[8–20] The increasing number of GPCR X-ray structures,[21,22] including the recently solved histamine H_1 receptor (H_1R) crystal structure[23] (Fig. 1A), offers new opportunities for histamine receptor homology modeling and the structure-based design of new histamine receptor ligands.[24–27] However, computational H_4R–ligand *binding mode* prediction still remains a challenging task. The symmetric distribution of the two acetic residues (aspartate $D94^{3.32}$ and glutamate $E182^{5.46}$)[2,3,7] in combination with different hydrophobic subpockets (I and II,[28] Fig. 1B and C) that are complementary to (two) basic and several hydrophobic groups in H_4R ligands (Fig. 2)[29–31] allows *different* plausible H_4R–ligand binding modes. Site-directed mutagenesis studies have identified $D94^{3.32}$ (a conserved binding residue in bioaminergic GPCRs)[32] as an essential residue in H_4R to bind both the non-imidazole antagonist JNJ 7777120 **1b**[3] and the small imidazole-containing agonist histamine **3**.[3,7] In addition, site-directed mutagenesis (SDM) studies showed that the anionic carboxylate group of $E182^{5.46}$ plays an important role in binding of H_4R ligands that contain two basic groups, including **3**, VUF 8430 **4**, and to a smaller degree clobenpropit **5** and clobenpropit analogue VUF 5228 **6**, while **1b** and clozapine **7** only require a H-bond acceptor at position $182^{5.46}$ (*e.g.* present in the $E182^{5.46}$Q mutant).[2,3] In the H_1R co-crystal structure[23] the inverse agonist doxepin forms an ionic H-bond interaction with the conserved $D107^{3.32}$, but does not form a H-bond with $N198^{5.46}$. The aromatic ring systems of doxepin bind to two connected subpockets in the hydrophobic cavity between transmembrane (TM) helices 3–6 (pocket II[28]), in the current study defined as *subpocket IIa* and *subpocket IIb* (Fig. 1A). Receptor mutagenesis, ligand SAR, and receptor–ligand interaction modeling studies have indicated that different ligands bind to these different subpockets.[2,4,30,33]

Ligands **6** and **7** occupy both subpockets IIa and IIb simultaneously (Fig. 1B and C).[2,4] Triazole ligand **8** is proposed to bind only in subpocket IIa,[33] while combined modeling and mutagenesis studies support two alternative binding modes of ligand **5** in which it accommodates its aromatic moiety in subpocket IIb, or, alternatively, in subpocket I.[2]

In this study we have focused on the elucidation of the binding interactions of two different selective H_4R ligand classes: indolecarboxamides[4,6,27,36–39] (**1a,b**) and 2-aminopyrimidines[40–46] (**2a,b**) (Fig. 2). Recent ligand-binding mode

[a]*Leiden/Amsterdam Center for Drug Research (LACDR), Division of Medicinal Chemistry, Department of Pharmacochemistry, Faculty of Exact Sciences, VU University Amsterdam, De Boelelaan 1083, 1081 HV Amsterdam, The Netherlands. E-mail: c.de.graaf@vu.nl*

[b]*Boehringer Ingelheim RCV GmbH & Co KG, Department of Medicinal Chemistry, Dr Boehringer-Gasse 5-11, Vienna, Austria*

† Electronic supplementary information (ESI) available: Additional analyses of molecular dynamics simulations, purity of compounds by LC-MS and NMR, and comparison of ADRB2 *vs.* H_1R crystal structure based H_4R homology models. See DOI: 10.1039/c2md20212c

‡ These authors contributed equally.

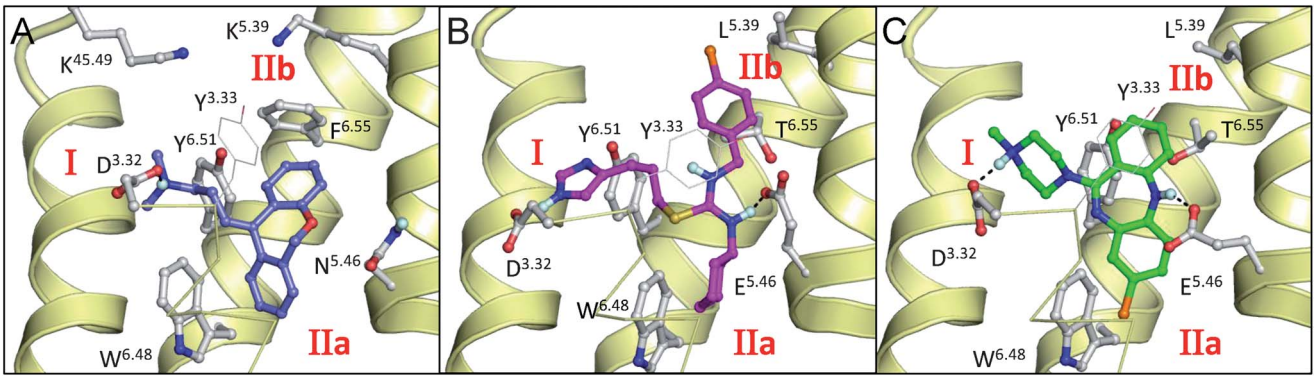

Fig. 1 Binding modes of doxepin in the H_1R co-crystal structure[23] (A), and clozapine[4] (B) and VUF 5228 (ref. 2) (C) in (ADRB2 crystal structure[34] based) H_4R homology models. Compounds and pocket residues are depicted as ball-and-sticks, whereas for clarity $Y95^{3.33}$ is shown as lines. H-bonds between the ligand and pocket residues are represented as black dotted lines. The backbone TM helices 5, 6, and 7 (right to left) are presented as yellow helices. Helix 3 is presented by yellow ribbons. Subpockets I, IIa and IIb are labeled in red.

predictions of dual H_3R/H_4R clobenpropit ligands **5** and **6** demonstrated that the integration of complementary *in vitro* and *in silico* modeling approaches is an efficient way to map protein–ligand interactions.[2] In the current study we used *in silico* guided mutation studies to compare the binding modes of substituted and unsubstituted indolecarboxamides and 2-aminopyrimidines. To obtain more detailed insights into ligand-specific molecular recognition features, molecular dynamics (MD) simulations were employed, a technique that has been successfully applied to describe subtle differences in ligand binding (*e.g.* ligand regio-, stereo-, and protein-selectivity[47,48]). Furthermore, different ligand protonation states (*i.e.* 2-aminopyrimidines **2a,b** with one *versus* two positively ionized basic groups) and different H_4R modeling templates (*i.e.* the bioaminergic GPCR β2-adrenergic receptor (ADRB2)[34] *versus* the more closely related H_1R)[23] were considered to investigate the influence of modeling parameters. The combination of protein mutagenesis data with different binding mode hypotheses, molecular modeling and MD-simulation revealed similarities as well as differences in the molecular H_4R binding determinants for both ligand classes. These insights are useful for rational optimization of indolecarboxamides and 2-aminopyrimidines, and the design of new H_4R ligands.

Results

SAR (Table 1, Fig. 3) and mutagenesis (Table 2, Fig. 4) studies in combination with docking and MD-simulations (Fig. 5–7, Tables 3 and 4) were used to elucidate the binding modes of indolecarboxamides **1a,b** and 2-aminopyrimidines **2a,b** (Fig. 2) in the H_4R binding site and to give insights into the molecular determinants of H_4R–ligand interactions. For this procedure different starting poses of the ligands were generated (Fig. 5) in different H_4R models (Fig. S1†). For the 2-aminopyrimidine ligands different protonation states were considered (Tables 3 and 4). The H_4R–ligand binding mode models that could best

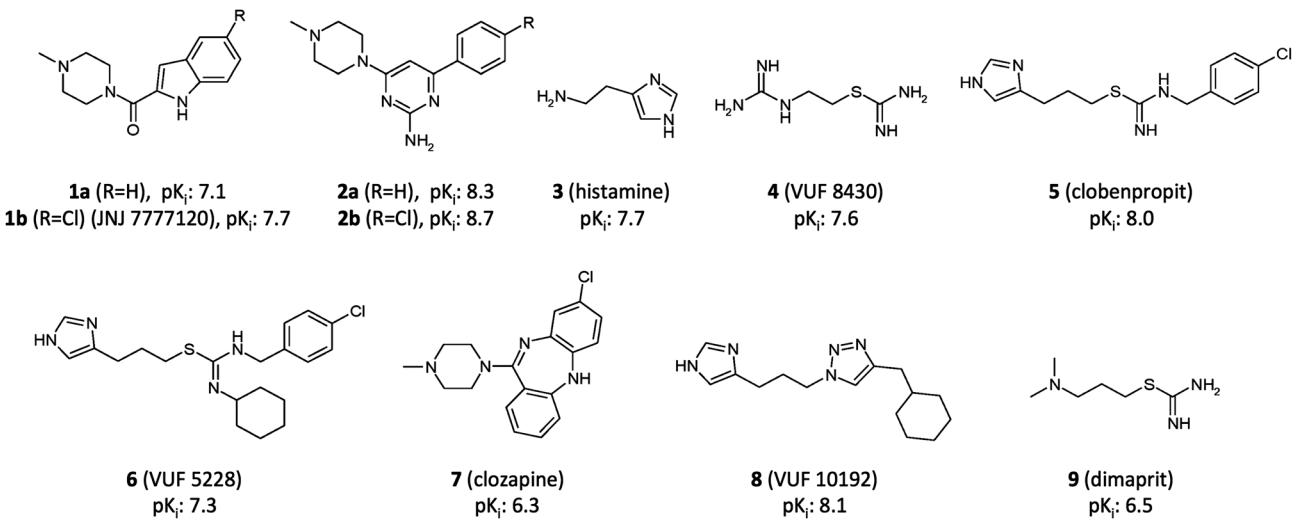

Fig. 2 Structures of H_4R ligands **1–9**. Affinities (pK_i) for H_4R of **1** and **2** are from the current study, **3**, **4** and **7** from ref. 4, **5** and **6** from ref. 2, **8** from ref. 33 and **9** from ref. 35.

Table 1 pK_i values of indolecarboxamides (1) and 2-aminopyrimidines (2) with different R substitutions[a]

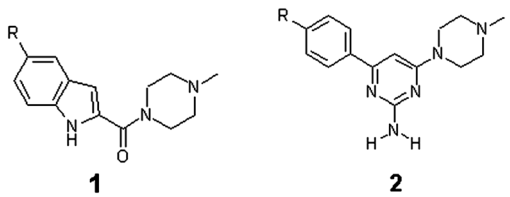

Ligands (R)	a (H)	b (Cl)	c (NH_2)	d (NO_2)	e (OCH_3)
1	7.1(0.07)	7.7(0.07)	7.6(0.10)	7.0(0.20)	5.3(0.16)
2	8.3(0.09)	8.7(0.15)	8.3(0.04)	8.1(0.00)	7.8(0.05)

[a] Data shown are mean of at least two independent experiments performed in triplicate (SEM given between brackets).

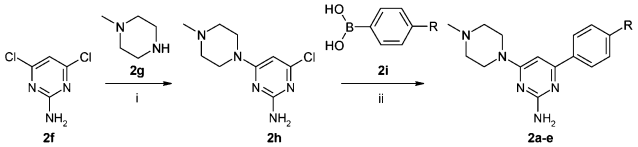

Fig. 3 *Reagents and conditions*: (i) dichloromethane, *N*-ethyl-diisopropylamine, 20 °C, 16 h; (ii) dichloro[1,1′-bis(diphenylphosphino)ferrocene]palladium(II) dichloromethane adduct, Cs_2CO_3, tetrahydrofuran, 1-methyl-2-pyrrolidinone, water, 100 °C, 16 h.

Table 2 pK_i values of ligands **1a,b** and **2a,b** for the H_4R, $L175^{5.39}V$ and $E182^{5.46}Q$[a]

Ligands	WT	$L175^{5.39}V$	$E182^{5.46}Q$
1a	7.1 (0.07)	6.5 (0.13)	6.7 (0.09)
1b	7.7 (0.07)	6.4 (0.07)	7.5 (0.08)
2a	8.3 (0.09)	7.7 (0.29)	7.2 (0.02)
2b	8.7 (0.15)	7.2 (0.12)	6.7 (0.15)

[a] Data shown are mean of at least two independent experiments performed in triplicate (SEM given between brackets).

explain the (ligand specific) mutation data were used to identify similarities and differences in the binding characteristics for the different ligand classes.

Structure–activity relationships of substituted indolecarboxamides and 2-aminopyrimidines

To determine the binding mode of indolecarboxamides and 2-aminopyrimidines we synthesized H, Cl, NH_2, NO_2, and OCH_3 substituted indolecarboxamide (**1a–e**) and 2-aminopyrimidine (**2a–e**) analogues and investigated the effect of different substituents for both ligand classes (Table 1). The synthesis of the indolecarboxamide ligands is described in the literature[36,37,39] and Fig. 3 illustrates the synthesis route for the 2-pyrimidine-2-amine derivatives. Starting from 4,6-dichloropyrimidine-2-amine, methylpiperidine was introduced *via* a

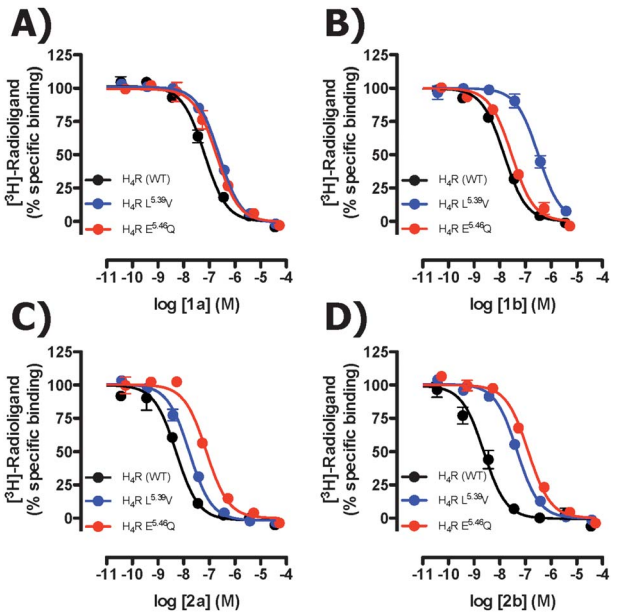

Fig. 4 Radioligand displacement curves of ligands **1a** (A), **1b** (B), **2a** (C), **2b** (D) on H_4R WT (●), H_4R-$L^{5.39}V$ (●), H_4R-$E^{5.46}Q$ (●). $E^{5.46}Q$ binding studies were performed with the radioligand [^{3}H]-JNJ 7777120, whereas [^{3}H]-histamine was used for H_4R and $L^{5.39}V$. Data shown are representative specific binding curves of at least two experiments performed in triplicate. Error bars indicate SEM values. To enable a better visualization of the pK_i shifts, each curve is corrected for the respective radioligand concentration and K_d values.

nucleophilic aromatic substitution reaction. In a second step the accordant phenyl moieties were installed using a Suzuki reaction.

Radioligand displacement studies of [^{3}H]-histamine binding to the human H_4R of the indolecarboxamide (**1a–e**) and 2-aminopyrimidine (**2a–e**) analogues indicated that the SAR of the two ligand series is comparable for small substituents but deviates for the larger –OCH_3 substituent (Table 1). Substitution of the indolecarboxamide with the methoxy group (**1e**) resulted in a 63-fold decrease compared to the unsubstituted ligand (**1a**), while comparison of the methoxy- (**2e**) and unsubstituted (**2a**) 2-aminopyrimidines gave only a 3-fold affinity change. The Cl-substituted ligands showed the highest H_4R binding affinity for both the indolecarboxamide and 2-aminopyrimidine ligand classes.

Ligand binding affinities for H_4R, $L175^{5.39}V$ and $E182^{5.46}Q$

The binding affinities (pK_i) of the unsubstituted and Cl-substituted indolecarboxamide and 2-aminopyrimidine ligands were analysed for H_4R, $L175^{5.39}V$ and $E182^{5.46}Q$ (Table 2, Fig. 4) using heterologous [^{3}H]histamine displacement binding experiments. Previous studies have shown that $E182^{5.46}Q$ affects the binding of H_4R ligands that contain two basic groups (**3–6**),[2,3,7] but does not affect binding of ligands that contain only one basic moiety (**1b**, 7).[3] The $L175^{5.39}V$ mutant affects the affinity for larger ligands **1b** and 7, but does not affect the binding of **3**.[4] The fact that these two mutants show ligand-dependent effects and that they have previously been used to

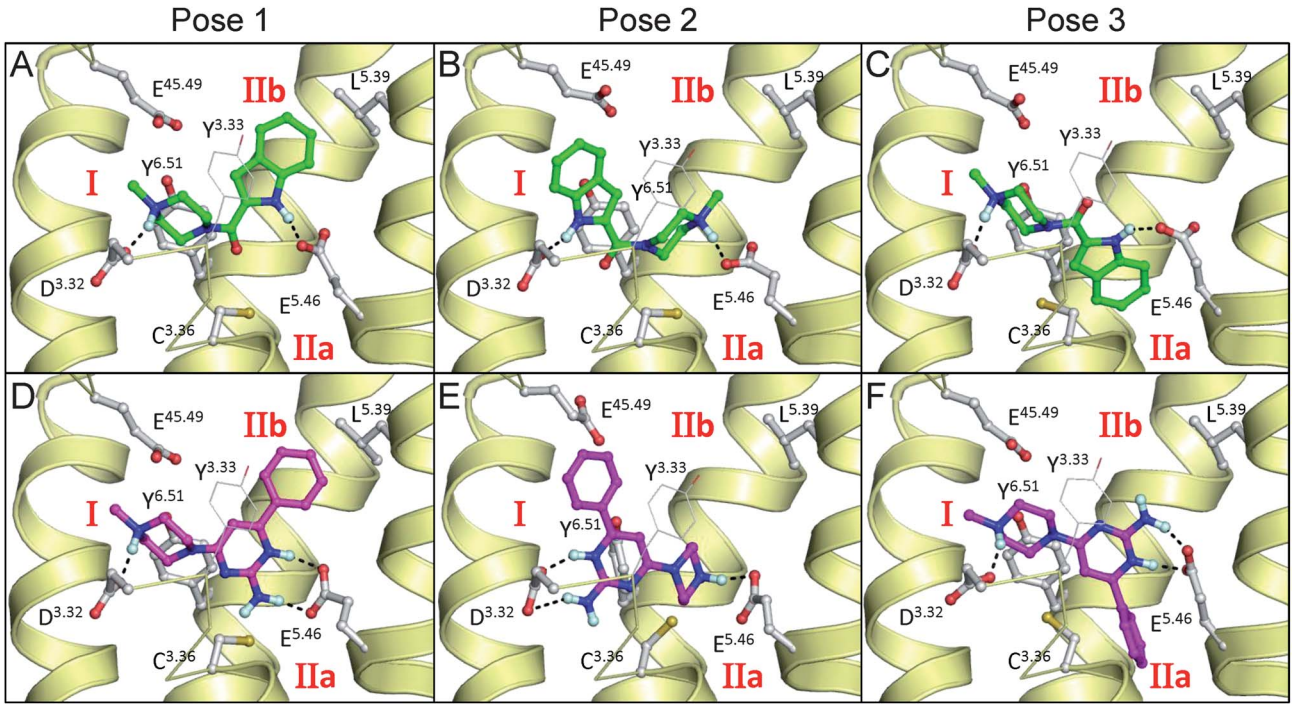

Fig. 5 Initial binding poses of indolecarboxamide ligand **1a** (A–C) and 2-aminopyrimidine ligand **2a** (D–F) in H_1R crystal structure based H_4R models used as starting structures for MD simulations. Rendering and labels are the same as in Fig. 1.

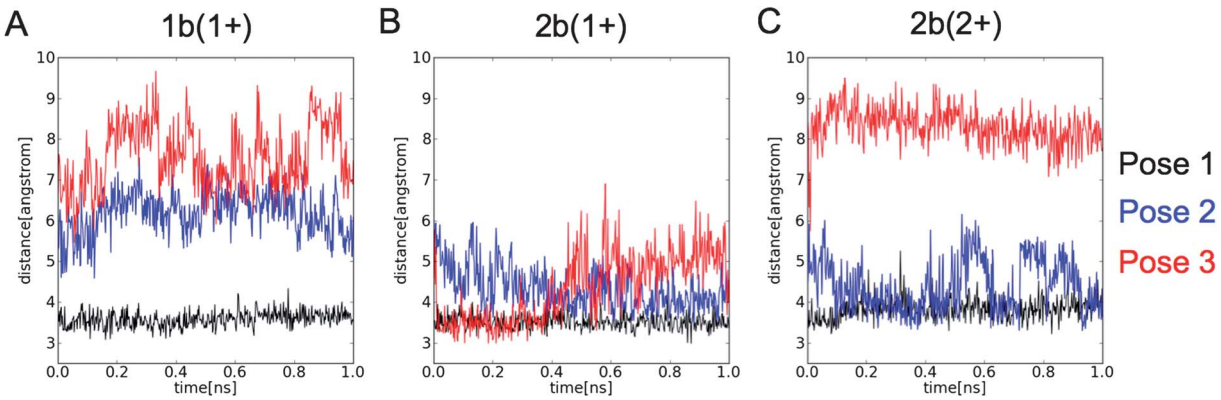

Fig. 6 Shortest distance between any heavy atom of the $L175^{5.39}$ and (A) **1b**, and (B) mono-protonated (1+) and (C) double-protonated (2+) **2b** in MD-simulations starting from pose 1 (black), pose 2 (blue), and pose 3 (red) (see Fig. 5).

investigate the binding mode of **1b** makes them attractive tools for investigating similarities and differences in binding modes of **1a,b** and **2a,b**. Both ligand classes lost affinity for $L175^{5.39}V$. The Cl-substituted ligands, **1b** and **2b**, were more affected (ΔpK_i(**1b**): −1.3, ΔpK_i(**2b**): −1.5) than the unsubstituted ligands, **1a** and **2a**, (ΔpK_i(**1a**): −0.6, ΔpK_i(**2a**): −0.6). In contrast, $E182^{5.46}Q$ had a different effect on the two ligand classes. While the affinities of the 2-aminopyrimidines for $E182^{5.46}Q$ significantly decreased (ΔpK_i(**2a**): −1.1, ΔpK_i(**2b**): −2) the mutations did not have a significant effect on the affinities of the indolecarboxamides (ΔpK_i(**1a**): −0.4, ΔpK_i(**1b**): −0.2). Again the Cl-substituted 2-aminopyrimidine ligand **2b** was more affected than the unsubstituted ligand **2a**.

Molecular docking studies

We used molecular docking simulations[49,50] to generate different plausible poses for the two indolecarboxamides (**1a** and **1b**) and 2-aminopyrimidines (**2a** and **2b**) in a H_4R homology model that is based on the recently resolved H_1R crystal structure (Fig. 5).[23] For comparison we also investigated docking poses in a H_4R model that is based on the ADRB2 crystal structure[34] (Fig. S1†) as this model was as good as the H_1R-based H_4R model in retrospective virtual screening studies.[51] While the TM helices of ADRB2 and H_1R crystal structures share the same overall fold,[23,34] the conformations of in particular the second extracellular loops (EL2) are different (Fig. S1†).

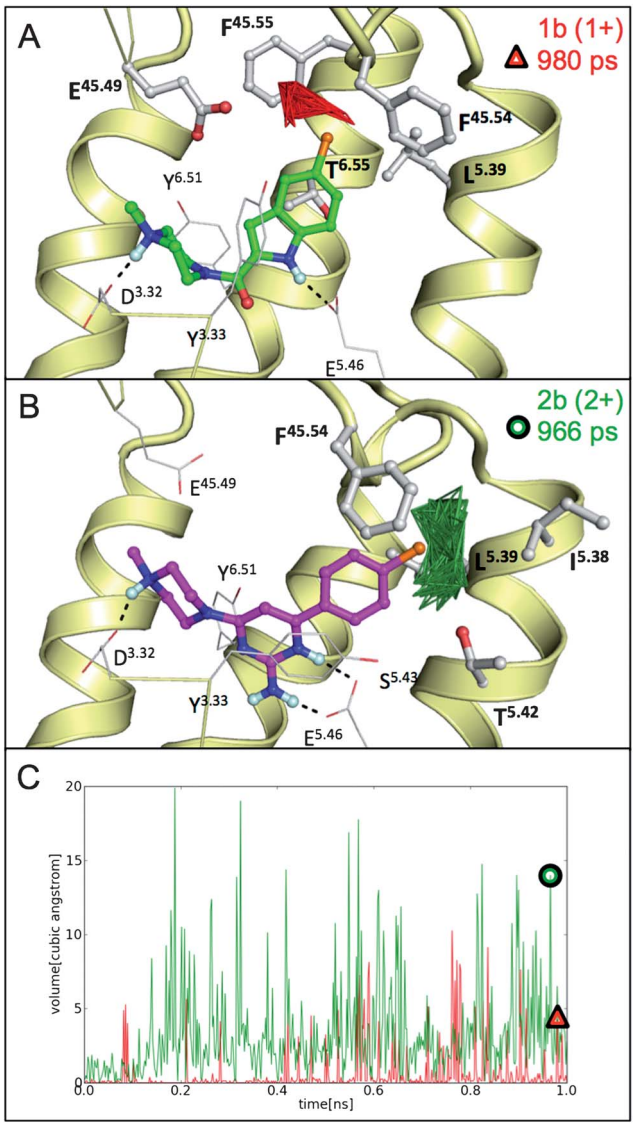

Fig. 7 Representative snapshots of MD simulations starting from pose 1 in the H_1R-based H_4R model showing the pocket volume within 3.5 Å of the chlorine atom of ligand **1b** (red, A) and ligand **2b** (green, B). The snapshots presented in panels A (red triangle) and B (green circle) are indicated in panel C, showing pocket volumes within 3.5 Å of the chlorine atom of ligand **1b** (red) and double-protonated ligand **2b** (green) along the full 1 ns MD trajectories.

As a result, the H_4R models based on ADRB2 and H_1R crystal structures have very similar TM domains and show overall the same receptor–ligand interactions, except in the EL2 loop region (Fig. S1†). Only docking poses where the ligands interact with both, aspartate $D94^{3.32}$ and glutamate $E182^{5.46}$ (essential residues for binding of H_4R ligands)[3,7] were considered. Both residues were modelled in the deprotonated (negatively charged) state. Three binding poses were generated for both ligand classes in the two different H_4R models as starting structures for MD simulations. The binding pose of indolecarboxamides in Fig. 5A (pose 1) is similar to the binding mode proposed by Lim *et al.*,[4] in which the piperazine and indole nitrogen atoms of the ligand donate H-bonds to $D94^{3.32}$ and $E182^{5.46}$, respectively, while the aromatic moiety of the ligand is accommodated in the upper hydrophobic subpocket IIb. The binding pose in Fig. 5B (pose 2) is similar to the pose proposed by Kiss *et al.*[38] in which the piperazine and indole nitrogen atoms of the ligand donate H-bonds to $E182^{5.46}$ and $D94^{3.32}$, respectively, while the aromatic moiety of the ligand is directed towards TM7 (subpocket I[28]). The binding pose in Fig. 5C (pose 3) is similar to the binding mode reported by Schneider *et al.*,[6] in which the piperazine and indole nitrogen atoms of the ligand donate H-bonds to $D94^{3.32}$ and $E182^{5.46}$, respectively (similar to pose 1), while the aromatic ring of the ligand binds to subpocket IIa. To obtain this latter pose the χ_1 torsional angle of $C98^{3.36}$ was rotated from its *t*-conformation to the *g+*-conformation.

Three docking poses were selected for the 2-aminopyrimidines that correspond to the respective poses of the indolecarboxamides (Fig. 5D–F). The amino group of the pyrimidine interacts in a similar manner as the NH of the indole group in these poses. A binding pose for 2-aminopyrimidines that is comparable to pose 1 was proposed by Werner *et al.*,[40–46] with the exception that the 2-aminopyrimidine moiety in the Werner H_4R model is differently oriented in the H_4R binding pocket and H-bonds to $E182^{5.46}$ are formed *via* water molecules.[40–46] The 2-aminopyrimidines can form an additional hydrogen bond with either $E182^{5.46}$, in pose 1 or 3, or $D94^{3.32}$ in pose 2 when the pyrimidine ring is protonated. pK_a measurements for ligand **2a** (see Experimental section for procedure) revealed a pK_a value of 7.5 for the piperazine nitrogen atom and a pK_a value of 6.0 for the pyrimidine, indicating that in solution approximately 2.3% of ligand **2a** will be double-protonated at physiological pH 7.4.

Molecular dynamics simulations

Binding mode elucidation. All three binding poses were subjected to 1 ns MD simulations. During the course of the MD-simulation 500 snapshots were collected. H-bond interactions between the ligands **1a,b** and **2a,b** and the carboxylate groups of $D94^{3.32}$ and $E182^{5.46}$, as well as hydrophobic contacts between the ligands and $L175^{5.39}$ were monitored (Table 3, Fig. 6) to validate the different binding mode models with mutagenesis data. Our data showed that the $E182^{5.46}$Q mutant affects binding of **2a** and **2b**, but not of **1a** and **1b**, while the $L175^{5.39}$V mutation affects the affinity of all ligands (Table 2 and Fig. 4). In addition, previous mutation studies[3,7,32,52,53] indicated that the conserved $D94^{3.32}$ residue plays an important role in histamine receptor binding, while an H-bond donor in the side-chain of residue $182^{5.46}$ in H_4R (*e.g.* present in the $E182^{5.46}$Q mutant) is required to bind **1b.**[3] Table 3 shows the frequency of hydrophobic contacts of the ligand with $L175^{5.39}$ *in combination* with H-bond formation with *both* $D94^{3.32}$ and $E182^{5.46}$ (Tables S1 and S2† report the individual and combined frequencies of the different interactions). Frequent interactions of indolecarboxamides (**1a** and **1b**) and 2-aminopyrimidines (**2a** and **2b**) with $L175^{5.39}$ in combination with stable H-bond formation with $D94^{3.32}$ and $E182^{5.46}$ were only observed in the MD-simulations starting from pose 1 (Table 3, Fig. 6). Starting from pose 2, only the MD-simulations of ligands **2a** and **2b** showed interactions with $L175^{5.39}$ in combination with H-bond

Table 3 Frequency (%) of hydrophobic interactions[a] between the ligand and L175$^{5.39}$ in combination with H-bond formation[b] with D94$^{3.32}$ and E182$^{5.46}$ in H_1R-based and ADRB2-based H_4R models that occur during 1 ns MD simulations

Structure	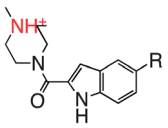		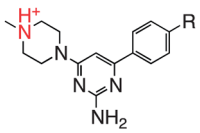		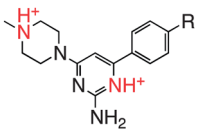	
Protonation	1+		1+		2+	
R	H	Cl	H	Cl	H	Cl
Name	**1a**	**1b**	**2a**	**2b**	**2a**	**2b**
H_1R based H_4R model						
Pose 1[c]	56.2	89.4	91.0	94.6	87.6	75.2
Pose 2[c]	0	0	15.4	14.4	22.6	24.0
Pose 3[c]	0	0	0	0	0	0
ADRB2 based H_4R model						
Pose 1[c]	21.0	70.6	90.2	80.0	51.2	88.8
Pose 2[c]	0	0	38.0	0	0.2	0
Pose 3[c]	0	0	0	0	0	0

[a] A hydrophobic interaction is counted if the shortest distance between any heavy atom of the ligand and L175$^{5.39}$ is ≤4 Å. [b] An H-bond is counted if the distance between the H-bond donor and acceptor heavy atom is below 3.5 Å and the angle between the H-bond donor heavy atom, hydrogen and H-bond acceptor heavy atom is between 135° and 225°. [c] See Fig. 5.

formation with D94$^{3.32}$ and E182$^{5.46}$, but the frequency of these interactions is much lower than in pose 1 (0–38% *vs.* 51–95%, Table 3), as demonstrated for ligand **2b** in Fig. 6B and C. In the ADRB2-H_4R model only for the mono-protonated ligand **2a** interactions with L175$^{5.39}$ (in combination with stable H-bonds with D94$^{3.32}$ and E182$^{5.46}$) were observed, but with significantly lower frequency (38%) than in pose 1 (90%, Table 3).

Protonation state elucidation of 2-aminopyrimidines bound to H_4R. Our mutagenesis studies (Table 2 and Fig. 3) showed that the affinities of indolecarboxamides were hardly affected by the E182$^{5.46}$Q mutation (ΔpK_i(**2a**): −0.4, ΔpK_i(**2b**): −0.2), while the affinities of the 2-aminopyrimidines were significantly affected by this mutation (ΔpK_i(**2a**): −1.1, ΔpK_i(**2b**): −2.0). These data indicate that ionic interactions with the negatively ionisable E182$^{5.46}$ residue play a role in binding of **2a** and **2b** (but not of **1a** and **1b**) and suggest that the basic 2-aminopyrimidine moieties of **2a-b** are protonated. To investigate this hypothesis, the mono and double-protonated **2a** and **2b** were modelled in E182$^{5.46}$Q mutated H_4R (pose 1) and subsequently subjected to MD simulations. As anticipated and shown in Table 4, only the H_4R binding models in which ligands **2a** and **2b** are *double-protonated* (*i.e.* both piperazine and

Table 4 Average H-bond interactions between the ligand and residue 182$^{5.46}$ in wild-type and E182$^{5.46}$Q H_4R models during 1 ns MD-simulation starting from pose 1 (see Fig. 5)

Structure		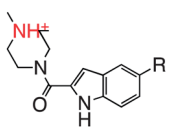		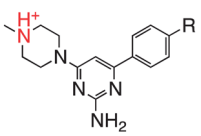		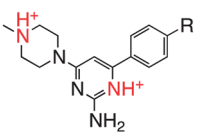	
Protonation		1+		1+		2+	
R		H	Cl	H	Cl	H	Cl
Name		**1a**	**1b**	**2a**	**2b**	**2a**	**2b**
H_1R based H_4R model							
WT	E$^{5.46}$	1.2	1.1	1.1	1.3	2.5	2.2
	D$^{3.32}$	0.9	0.9	1.0	1.0	1.0	1.0
E$^{5.46}$Q	Q$^{5.46}$	1.0	1.0	1.0	0.7	0.6	0.3
	D$^{3.32}$	1.0	0.9	0.1	0.6	1.0	0.9
ADRB2 based H_4R model							
WT	E$^{5.46}$	1.0	1.2	1.1	1.3	2.3	2.4
	D$^{3.32}$	1.0	1.0	1.1	1.2	1.0	1.0
E$^{5.46}$Q	Q$^{5.46}$	0.9	1.2	1.3	1.4	1.1	0.7
	D$^{3.32}$	1.0	1.0	1.0	1.0	1.0	1.0

aminopyrimidine groups in their positively ionized forms) can explain the observed affinity decrease for **2a** and **2b** upon E182$^{5.46}$Q mutation (Table 2). In these models the average number of hydrogen bonding interactions with residue 182$^{5.46}$ observed in the 500 snapshots was decreased in the E182$^{5.46}$Q mutant compared to the H_4R (difference in H-bond formation with 182$^{5.46}$ in H_1R–H_4R: **1a**(2+): −1.9, **1b**(2+): −1.9), ADRB2-H_4R: **2a**(2+): −1.2, **2b**(2+): −1.7), while H-bond interactions with D94$^{3.32}$ were unaffected. To compare the two ligand classes, also indolecarboxamides **1a** and **1b** in the E182$^{5.46}$Q models were subjected to 1 ns MD-simulation. In both E182$^{5.46}$Q models H-bond interactions with **1a** and **1b** were hardly affected compared to the H_4R models (Table 4). This is in line with the fact that the E182$^{5.46}$Q mutation had no significant effect on binding affinity for these ligands (Table 2, Fig. 4).

Rationalization of differences in ligand structure–activity relationships

The SAR for different substitutions in both ligand series (Table 1) indicated that the larger substituent –OCH_3 is less compatible with the H_4R binding site than smaller apolar (–Cl) or polar (–NH_2, –NO_2) groups. This affinity decrease was much more pronounced for the indolecarboxamides than for 2-aminopyrimidines (Table 1). To explain this effect we monitored the pocket volume around 3.5 Å distance of the chlorine atom for **1b** and **2b** (Fig. 7). We observed that in the H_1R-based H_4R model the chlorine atom of **2b** (independent of the modeled protonation state) occupies more frequently larger pockets than the chlorine atom of **1b**. Average pocket volumes around the chlorine atom in the H_1R-based H_4R model were significantly *smaller* for ligand **1b** (0.6 Å^3) than for ligand **2b** (8.4 Å^3 (mono-protonated) and 3.2 Å^3 (double-protonated)) while in the ADRB2-based H_4R model the volume for **1b** (11.0 Å^3) was significantly *larger* than for **2b** (6.4 Å^3 (mono-protonated) and 3.9 Å^3 (double-protonated)). The H_1R-based H_4R models therefore explain the fact that 2-aminopyrimidines can accommodate larger substituents than indolecarboxamides. A comparison of representative snapshots at the end of the MD-simulation showed that although the overall orientation of the ligands in the binding pocket is comparable, the chlorine atoms of both ligands are oriented in different pockets (Fig. 7A and B). The chlorine atom of **1b** is directed towards the extracellular loop (EL2) and TM6 (surrounded by F168$^{45.54}$, F169$^{45.55}$, E163$^{45.49}$, L175$^{5.39}$, T323$^{6.55}$) in a relatively tight binding pocket (Fig. 7A). The chlorine atom of **2b** occupies a pocket, which is located more towards TM5 (surrounded by I174$^{5.38}$, L175$^{5.39}$ and T178$^{5.42}$ in TM5, as well as F168$^{45.54}$ and backbone atoms of EL2) and has a larger volume (Fig. 7B) that allows larger substituents (Table 1).

Discussion

In the current study, ligand SAR and H_4R SDM studies were combined with molecular docking and MD simulations to elucidate the binding modes of indolecarboxamides and 2-aminopyrimidines in the H_4R binding pocket. Insights were obtained into the similarities and differences of molecular interactions between H_4R and these two ligand classes.

Overlap in indolecarboxamides and 2-aminopyrimidines binding modes

Our combined SDM and *in silico* studies indicate that the binding modes of indolecarboxamides and 2-aminopyrimidines overlap, but also show that there are subtle differences in the importance of different H_4R interaction features within these two ligand series. Ligands of both ligand classes accommodate their aromatic ring moieties in subpocket IIb that is located in the upper half of the extracellular regions between TM helices 3–6 (pose 1), (Fig. 5A and D and Fig. S1†). Only in this pose all ligands (**1a,b** and **2a,b**) form stable H-bond interactions with D94$^{3.32}$ and E182$^{5.46}$ in combination with hydrophobic interactions with L175$^{5.39}$. Current (Table 2 and Fig. 4) and previous SDM studies show that these interactions are important binding determinants for ligands **1a,b** and **2a,b** as well as other H_4R ligands.[2,3,7] The overall binding orientation was stable and not influenced by interactions with water molecules.

It should be noted that effects of H_4R mutations are often ligand specific. While the E182$^{5.46}$Q mutant has a decreased affinity for ligands **2a**, **2b**, **3**, and **4**, this mutation does not affect binding of ligands **1a**, **1b** and **7** (Table 2 and Fig. 4).[2,3] The L175$^{5.39}$V mutant that mimics the monkey H_4R has a decreased affinity for **1** and **2** (Table 2 and Fig. 4) but an increased affinity for ligand **7** (Fig. 1B), while binding of ligand **3** is not affected by this mutation.[4] This reflects the diversity in H_4R ligand binding modes (Fig. 1 and 7) that can match different parts of the H_4R ligand pharmacophore.[30] This pharmacophore contains: (i) 1 to 2 H-bond donors (*e.g.* piperazine and indole/aminopyrimidine nitrogen atoms of ligands **1** and **2**) that are complementary to D94$^{3.32}$ (ref. 3 and 7) and E182$^{5.46}$, (ii) a central *aromatic* moiety (*e.g.*, indole (**1**) and 2-aminopyrimidine (**2**) moieties) that stacks between Y$^{3.33}$ and Y$^{6.51}$, and (iii) 1 to 2 hydrophobic moieties that can accommodate subpockets IIa (*e.g.*, cyclohexyl groups of ligands **6** (Fig. 1C) and **8**, the chlorinated benzene ring of ligand **7** (Fig. 1B)),[2,4,33] IIb (benzene rings of ligands **1** and **2** (Fig. 7) and ligands **5** and **-7** (Fig. 1B and C)[2,4] between TM helices **3–6**, or alternatively, subpocket I between TM helices **3** and **5–7** (benzene ring of ligand **5**).[2]

Our MD-simulation showed that although the overall orientation of the ligands (**1a,b** and **2a,b**) in the H_4R binding pocket is comparable, the chlorine atoms of indolecarboxamide and 2-aminopyrimidine ligands are located in subpockets of different size (Fig. 7). This size difference explains why larger substituents have a more negative effect on the affinity for indolecarboxamides than for 2-aminopyrimidines (Table 1). Interestingly, SDM studies have shown ligand-dependent effects towards mutations in the same EL2 region that can explain H_4R species selectivity differences.[5]

The role of ligand protonation states in H_4R binding

In silico evaluation of different protonation states of 2-aminopyrimidines showed that the H_4R binding models in which *both*

the piperazine and 2-aminopyrimidine moieties are positively ionized best explain the affinity decrease of ligands **2a** and **2b** (but not of **1a** and **1b**) for the E182$^{5.46}$Q mutant (Tables 2–4). The pK_a value of the pyrimidine ring of 6.0, however, suggests that under physiological pH 7.4 only a small portion (~2.3%) of ligands **2a** and **2b** contains a positively ionized pyrimidine ring. On the other hand, it has been reported that pK_a values of functional groups in ligands can change upon binding, as demonstrated for the pteridine ring of methotrexate that becomes protonated upon binding to dihydrofolate reductase.[54,55] Thus, it cannot be excluded that the pK_a value of the 2-aminopyrimidine ring is shifted towards higher values upon binding to H_4R.

It should furthermore be noted that also other ligands have been proposed to bind in a double-protonated state to H_4R. The two basic groups of ligand **9** have pK_a values of 8.3 and 9.4 (ref. 56) indicating that most parts of this ligand will be double-protonated at pH 7.4. Agonist **4** (ref. 57), derived from ligand **9**, has two chemically similar basic moieties, while the pK_a values of the amine and imidazole groups of **3** (9.4–9.9 and 5.9–6.5, respectively)[58–60] suggest that also **3** might bind in a double-protonated form. This is supported by the fact that the E182$^{5.46}$Q H_4R mutant has a significantly decreased affinity for small agonists **3** and **4** (ref. 3) that depend on strong H-bond interactions. The effects of the E182$^{5.46}$Q mutation on H_4R binding affinity are relatively smaller (**5** and **6**) or not significant (**1a,b** and **7**) for ligands with larger hydrophobic moieties (Table 2, Fig. 4),[2,3] as the binding of these molecules is more determined by hydrophobic interactions. Interestingly, in this current study we show that also the 2-aminopyrimidines (containing a hydrophobic benzene ring) are to a large extend dependent on ionic interactions with E182$^{5.46}$.

Ligand-binding mode predictions in H_4R homology models were modelling template independent

To elucidate H_4R-ligand binding modes we considered two H_4R models, one based on the ADRB2 crystal structure[34] and another based on the more recent H_1R crystal structure.[23] The ADRB2 and H_1R crystal structures share a similar fold[23] and consequently both models are constructed using the same modeling approach.[2,4] It is therefore not surprising that the overall structure of the homology models is relatively similar, and gives comparable results in ligand-binding mode prediction[2] and virtual screening studies.[51] Also in the current study, the conformational ensembles derived from MD simulations of ADRB2- and H_1R-based H_4R models show the same overall binding mode (pose 1) for indolecarboxamides and 2-aminopyrimidines that matches our SDM studies (Table 2 and Fig. 4).

In contrast, only the H_1R-based H_4R model is able to explain that larger substituents have a larger negative effect on the affinity for indolecarboxamides than for 2-aminopyrimidines (Table 1) because the chlorine atoms of indolecarboxamide and 2-aminopyrimidine ligands are located in different subpockets close to EL2 (as discussed above). Accurate GPCR loop modelling is still very challenging, as demonstrated by the recent GPCR DOCK competitions to predict the coordinates of GPCR–ligand co-crystal structures,[61,62] and emphasized by the different extracellular loop structures displayed in the currently available GPCR crystal structures.[21,63] Despite some recent reports of successful automated retrospective prediction of individual loops of GPCR crystal structures,[64] GPCR loop modeling should be approached with much caution and should be reserved for cases where loop building can be guided and validated by experimental data.[65] Moreover, structure-based virtual screening studies have shown that *loopless* TM models of GPCRs can be suitable targets for virtual screening as well.[63] Nevertheless, our H_4R modeling studies indicate that the crystal structure of the more closely related H_1R provides a better template for the EL2 region (despite the fact that some parts of this loop were not resolved in the H_1R crystal structure),[23] and to construct H_4R models that can describe subtle differences between ligand binding modes.

Docking in combination with MD simulations explains H_4R mutation studies

In particular the symmetric distributions of two acetic residues (aspartate D94$^{3.32}$ and glutamate E182$^{5.46}$) and two hydrophobic subpockets IIa and IIb that are complementary to (two) basic and several hydrophobic groups in H_4R ligands allow *different* plausible binding H_4R–ligand modes (Fig. 5). Previous[66] and current studies suggest that molecular docking alone is not suitable for accurate determination of relative probabilities of different ligand binding modes. To explain the *in vitro* SDM data (Table 2, Fig. 4), which are an average of different ligand and receptor orientations with time, a dynamic treatment of both ligand and receptor is required (Tables 3 and 4). MD simulations can account for distributions of protein–ligand interactions and thus can give a more comprehensive explanation of ligand-dependent mutation effects (Tables 2–4) and subtle differences in ligand structure–activity relationships (Table 1, Fig. 7).[67,68] By systematically considering different ligand binding mode hypotheses and protein models, and combining ligand SAR and protein mutagenesis experiments with extensive MD-simulation studies (48 independent MD runs in total) we could identify similarities and differences in the molecular determinants of H_4R binding for both indolecarboxamide and 2-aminopyrimidine ligand classes.

Conclusion

We have successfully combined complementary *in silico* H_4R structural modeling approaches and ligand SAR with *in vitro* mutagenesis data to investigate the binding mode of indolecarboxamides and 2-aminopyrimidines in H_4R. By systematically considering different H_4R modelling templates, ligand binding poses, and ligand protonation states in combination with molecular docking and MD simulations we are able to explain ligand-specific mutation effects and subtle differences in ligand SAR. Our results improve the knowledge of H_4R–ligand binding and provide valuable information for optimizing and developing other H_4R-specific ligands. The combined *in silico* modelling and *in vitro* SAR and mutagenesis approach

presents a promising approach to explore protein–ligand interactions and can be considered as a general method to elucidate protein ligand-binding modes.

Experimental section

Synthetic methods

General remarks. Chemicals and reagents were obtained from commercial suppliers and were used without further purification. Proton and carbon NMR spectra were obtained on a Bruker Advance 400 FT-NMR or Bruker Advance 500 FT-NMR instrument with chemical shifts (δ) reported relative to tetramethylsilane as an internal standard.

High resolution mass spectroscopy data were obtained on a LTQ Orbitrap XL (Thermo Scientific) equipped with a NSI Source (Advion Nanomate) in ESI positive mode.

Analytical HPLC-MS analyses were conducted using an Agilent 1100 series LC/MSD system. The analytic method A1 is defined in Table S3.† Ligand purities were calculated as the percentage peak area of the analyzed ligand by UV detection at 254 nm. If purity data are not explicitly mentioned the ligand displays a purity >95%. Flash column chromatography was carried out using hand packed silica gel 60 (230–400 mesh) or pre-packed silica gel columns from Biotage and the product was eluted under medium pressure liquid chromatography. Preparative high performance chromatography was carried out on a Gilson system (pump system: 333 and 334 prep-scale HPLC pump; fraction collector: 215 liquid handler; detector: Gilson UV/VIS 155) using pre-packed reversed phase silica gel columns from waters. The method for preparative high performance chromatography P1 is defined in Table S3.†

*6-Chloro-4-(4-methylpiperazin-1-yl)pyrimidin-2-amine (**2h**).* 4,6-Dichloro-pyrimidine-2-amine **2f** (1.00 g, 5.79 mmol), *N*-ethyl-diisopropylamine (1.33 g, 11.58 mmol) and 1-methylpiperazine **2g** (0.64 g, 6.37 mmol) were suspended in 30 ml dichloromethane and stirred for 16 h at 20 °C. The solvent was removed under reduced pressure and the crude material was purified using silica gel flash column chromatography with a solvent mixture of dichloromethane, methanol and 25% aqueous ammonia of 90 : 9 : 1 for elution. The solvent of the corresponding fractions was evaporated under reduced pressure, yielding 0.9 g (70%) of the title ligand. Purity by method A1: >95%; RT = 1.01 min; MS (ESI^+) *m*/*z* 228/230 $[M + H]^+$, Cl distribution; HRMS (ESI^+) *m*/*z* found 228.1015 $[M + H]^+$, $C_9H_{15}ClN_5$ requires M^+ 228.1016; ^1H NMR (DMSO) δ (ppm) 6.45 (s, 2H), 6.08 (s, 1H), 3.56–3.47 (m, 4H), 2.30 (t, J = 5.1 Hz, 4H), 2.19 (s, 3H).

*4-phenyl-6-(4-methylpiperazin-1-yl)pyrimidin-2-amine (**2a**).* 4-Chloro-6-(4-methylpiperazin-1-yl)pyrimidin-2-amine **2h** (100 mg, 0.44 mmol), 2-phenylboronic acid (66 mg, 0.53 mmol), caesium carbonate (286 mg, 0.88 mmol) and dichloro[1,1′-bis(diphenylphosphino)ferrocene]palladium(II) dichloromethane adduct (36 mg, 0.04 mmol) were suspended in 1 ml of a 3 : 1 : 1 mixture of tetrahydrofuran, 1-methyl-2-pyrrolidinone and water. The reaction mixture was flushed with argon and stirred for 16 h at 100 °C. The crude product was purified using method P1, yielding 76 mg (64%, 0.28 mmol) of the title ligand. Purity by method A1: >95%; RT = 1.35 min; MS (ESI) *m*/*z* 270 $[M + H]^+$; HRMS (ESI^+) *m*/*z* found 270.1715 $[M + H]^+$, $C_{15}H_{20}N_5$ requires M^+ 270.1718; ^1H NMR (500 MHz, DMSO) δ (ppm) 8.05–8.01 (m, 2H), 7.45–7.41 (m, 3H), 6.57 (s, 1H), 6.06 (s, 2H), 3.64–3.59 (m, 4H), 2.37–2.34 (m, 4H), 2.21 (s, 3H).

Using the same method **2b–e** were synthesized. Analytic data for these ligands are given in the ESI.†

Pharmacological assays

Cell culture, transfection and membrane preparation. HEK293T cells were cultured in Dulbecco's modified Eagles medium (DMEM) supplemented with 10% fetal bovine serum (FBS), 50 IU ml^{-1} penicillin and 50 μg ml^{-1} streptomycin at 37 °C/5% CO_2. One day prior to transfection, the HEK293T cells were seeded at 2 × 10^6 cells per 10 cm dish. The polyethyleneimine (PEI) transfection method was used to transiently transfect HEK293T cells with H_4R, $L175^{5.39}V$ or $E182^{5.46}Q$ cDNA. Briefly, for each 10 cm dish 2.5 μg H_4R (mutant) cDNA and 2.5 μg pcDEF3 (empty vector) were incubated with 20 μg 25 kDa linear PEI in a total volume of 500 μl 150 mM NaCl for 30 minutes at room temperature. The transfection mix (cDNA–PEI mix) was subsequently added drop wise to the 10 cm dish with 6 ml fresh culture medium. Two days post transfection, cells were washed once with phosphate-buffered saline (PBS) and subsequently scraped from their culture dish in 1 ml of PBS. Crude membrane extracts were collected by centrifugation at ~2000*g* for 10 min at 4 °C. The crude membrane extract pellets were stored at −20 °C until further use.

Site-directed mutagenesis. The construction of the H_4R-$L175^{5.39}V$ and H_4R-$E182^{5.46}Q$ mutants has been previously described.[3,4]

[^{3}H]-Radioligand binding assay. The displacement binding assays were performed using crude membrane extracts from transiently transfected HEK293T cells in 50 mM Tris–HCl binding buffer (pH 7.4 at room temperature). Crude membrane extracts were co-incubated with the 2-aminopyrimidine or indolecarboxamide ligands (Table 1) and ~10 nM radioligand ([^{3}H]-histamine for H_4R-WT and H_4R-$L175^{5.39}V$ or [^{3}H]-JNJ 7777120 for H_4R-$E182^{5.46}Q$) in a total volume of 100 μl per well. The ligand–membrane mixtures were incubated for 1.5 h at room temperature on a shaking table (750 rpm). Bound radioligands were separated from free radioligands *via* rapid filtration over a 0.3% PEI-pre-soaked glass fiber C plate (GF/C, Perkin Elmer). GF/C plates were subsequently washed three times with ice-cold 50 mM Tris–HCl wash buffer (pH 7.4 at 4 °C). The retained radioactivity on the GF/C plates was counted by liquid scintillation counting in a Wallac Microbeta (Perkin Elmer).

Materials. [^{3}H]-Histamine (10.6–13.4 Ci $mmol^{-1}$) was purchased from Perkin Elmer and [^{3}H]-JNJ 7777120 (56.1 Ci $mmol^{-1}$) was a kind gift of Robin Thurmond (JNJ, La Jolla, CA). PEI was bought from Polysciences and cell cultures media were obtained from PAA (Pasching, Austria).

pK_a Measurements. For pK_a measurements a GLpKa automated pK_a analyser (Sirius Analytical Instruments Ltd) was used with standard methods described by Allen *et al.*[69] and Volgyi *et al.*[70]

Computational methods

H_4R model. The construction of the ADRB2-H_4R model has been described previously.[2,4] The H_1R-H_4R model was built in the same manner. The mutated H_4R model ($E182^{5.46}Q$) was constructed by mutating the corresponding residues of the H_4R model with the mutate function in MOE 2009.10.[71] The H_4R model was used either with the χ_1 torsional angle of $C98^{3.36}$ in the *t*-conformation or in the *g*+-conformation, where an additional pocket is assessable. Ligands were docked into both H_4R models using PLANTS[49,50] without restraints. As aspartate $D94^{3.32}$ and glutamate $E182^{5.46}$ are reported to be important for binding,[3,4] only docking poses where the ligands interact with both of these residues were selected.

Molecular dynamics simulations. The protein–ligand complexes were minimized using Amber10,[72] including restraints for the experimentally supported hydrogen bond interactions with aspartate $D94^{3.32}$ and glutamate $E182^{5.46}$ (ref. 3 and 4) (distance between the donor and acceptor atom and angle between the donor, hydrogen and acceptor atom). The number of H-bond interactions between ligands and the $E182^{5.46}$ side chain were generally low for all ligands in MD simulations in which the carboxylate group of $E182^{5.46}$ was considered in the (neutral) protonated state. This is not in line with the ligand-dependent effects of the $E^{5.46}Q$ mutation and therefore both residues were modelled in the deprotonated (negatively charged) state. The minimized protein–ligand complex was refined by a second minimization without restraints. The minimized complex was embedded in a pre-equilibrated lipid bilayer consisting of 1-palmitoyl-2-oleoyl-phosphatidylcholine (POPC) molecules and solvated with TIP3P water molecules as described by Urizar *et al.*[73] The whole complex was again minimized using restraints for the expected hydrogen bonds. Additionally positional harmonic restraints of 10 kcal mol^{-1} on Cα atoms of the helical domains of the H_4R receptor were applied during this minimization step. Each minimization was performed using a certain number of steps steepest descent followed by conjugate gradient until the root mean square gradient of the potential energy was lower than 0.0001 kcal mol^{-1}. Non-bonded interactions were calculated within a cut-off of 10 Å.

The entire system was subjected to a constant pressure (1 bar) MD-simulation. All bonds involving hydrogen atoms were frozen with the SHAKE algorithm. In the first 100 ps the temperature was increased in a stepwise manner to 300 K. During this procedure positional harmonic restraints on helical Cα atoms of 10 kcal mol^{-1} were applied which were reduced to 0.5 kcal mol^{-1} for the subsequent 1 ns production run (at 300 K). The temperature was controlled using the weak coupling approach[74] with a coupling constant of 0.2 ps. For calculating the long range electrostatic interactions the Particle Mesh Ewald (PMW) method was applied. van der Waals interactions were calculated within a cut-off of 8 Å.

For the protein, the POPC and the water molecules the AMBER03 force field[75] was used. For the ligand atoms the GAFF[76] force field was used. Ligand force field parameters were derived using ANTECHAMBER.[77] These parameters were adjusted and extended for 2-aminopyrimidine ligands to retain the amino group (and in the case of double protonation also the additional proton on the pyrimidine ring) in the plane of the pyrimidine ring. Partial charges for the ligand were derived using the AM1-BCC procedure in ANTECHAMBER. The tLEaP module of AMBER10 was used to generate the topology and coordinate files of the protein–ligand complex.

During the MD-simulation trajectories of every 1000^{th} MD-step were saved. This results in 500 snapshots for a 1 ns MD-simulation. Using the PTRAJ module of AMBER10 distances and angles could be extracted which were used to analyse H-bond interactions between the protein and the ligand and interactions of the ligand with $L175^{5.39}$. An H-bond was counted if the distance between the H-bond donor and acceptor was below 3.5 Å and the angle between the H-bond donor, hydrogen and H-bond acceptor was between 180 ± 45°.[78] Hydrophobic interactions of the ligand with $L175^{5.39}$ were counted if the distance between any heavy atom of the ligand and $L175^{5.39}$ was ≤4 Å.

Calculation of the pocket volumes. The pocket volume around the chlorine atoms of ligands **1b** and **2b** was determined using POVME.[79] A radius of 3.5 Å was chosen for the calculations. The chlorine atom in the pdb snapshots taken during the MD-simulation was deleted for these calculations. Padding was on a standard value of 1.09. This is the radius of a hydrogen atom. Basically, only the volume of the binding site that can be occupied by hydrogen atoms was measured. As the van der Waals radius of the carbon atom (where the chorine atom is attached to) and the diameter of a hydrogen atom overcome the diameter of the chlorine atom also pocket volumes of 0 $Å^3$ can be observed.

Acknowledgements

This research was financially supported by The Netherlands Organization for Scientific Research [NWO VENI Grant 700.59.408 to C. de G.], and COST Action BM0806. Obbe Zuiderveld is acknowledged for technical assistance.

References

1 P. Igel, R. Geyer, A. Strasser, S. Dove, R. Seifert and A. Buschauer, *J. Med. Chem.*, 2009, **52**, 6297–6313.
2 E. P. Istyastono, S. Nijmeijer, H. D. Lim, A. van de Stolpe, L. Roumen, A. J. Kooistra, H. F. Vischer, I. J. de Esch, R. Leurs and C. de Graaf, *J. Med. Chem.*, 2011, **54**, 8136–8147.
3 A. Jongejan, H. D. Lim, R. A. Smits, I. J. de Esch, E. Haaksma and R. Leurs, *J. Chem. Inf. Model.*, 2008, **48**, 1455–1463.
4 H. D. Lim, C. de Graaf, W. Jiang, P. Sadek, P. M. McGovern, E. P. Istyastono, R. A. Bakker, I. J. de Esch, R. L. Thurmond and R. Leurs, *Mol. Pharmacol.*, 2010, **77**, 734–743.
5 H. D. Lim, A. Jongejan, R. A. Bakker, E. Haaksma, I. J. de Esch and R. Leurs, *J. Pharmacol. Exp. Ther.*, 2008, **327**, 88–96.
6 E. H. Schneider, A. Strasser, R. L. Thurmond and R. Seifert, *J. Pharmacol. Exp. Ther.*, 2010, **334**, 513–521.
7 N. Shin, E. Coates, N. J. Murgolo, K. L. Morse, M. Bayne, C. D. Strader and F. J. Monsma, Jr, *Mol. Pharmacol.*, 2002, **62**, 38–47.

8 G. Coruzzi, M. Adami, E. Guaita, I. J. de Esch and R. Leurs, *Eur. J. Pharmacol.*, 2007, **563**, 240–244.
9 J. M. Cowden, J. P. Riley, J. Y. Ma, R. L. Thurmond and P. J. Dunford, *Respir. Res.*, 2010, **11**, 86.
10 P. J. Dunford, N. O'Donnell, J. P. Riley, K. N. Williams, L. Karlsson and R. L. Thurmond, *J. Immunol.*, 2006, **176**, 7062–7070.
11 P. J. Dunford, K. N. Williams, P. J. Desai, L. Karlsson, D. McQueen and R. L. Thurmond, *J. Allergy Clin. Immunol.*, 2007, **119**, 176–183.
12 F. Gantner, K. Sakai, M. W. Tusche, W. W. Cruikshank, D. M. Center and K. B. Bacon, *J. Pharmacol. Exp. Ther.*, 2002, **303**, 300–307.
13 C. L. Hofstra, P. J. Desai, R. L. Thurmond and W. P. Fung-Leung, *J. Pharmacol. Exp. Ther.*, 2003, **305**, 1212–1221.
14 G. C. Hsieh, P. Chandran, A. K. Salyers, M. Pai, C. Z. Zhu, E. J. Wensink, D. G. Witte, T. R. Miller, J. P. Mikusa, S. J. Baker, J. M. Wetter, K. C. Marsh, A. A. Hancock, M. D. Cowart, T. A. Esbenshade, J. D. Brioni and P. Honore, *Pharmacol., Biochem. Behav.*, 2010, **95**, 41–50.
15 H. D. Lim, R. A. Smits, R. Leurs and I. J. De Esch, *Curr. Top. Med. Chem.*, 2006, **6**, 1365–1373.
16 P. Ling, K. Ngo, S. Nguyen, R. L. Thurmond, J. P. Edwards, L. Karlsson and W. P. Fung-Leung, *Br. J. Pharmacol.*, 2004, **142**, 161–171.
17 C. Liu, X. Ma, X. Jiang, S. J. Wilson, C. L. Hofstra, J. Blevitt, J. Pyati, X. Li, W. Chai, N. Carruthers and T. W. Lovenberg, *Mol. Pharmacol.*, 2001, **59**, 420–426.
18 M. O'Reilly, R. Alpert, S. Jenkinson, R. P. Gladue, S. Foo, S. Trim, B. Peter, M. Trevethick and M. Fidock, *J. Recept. Signal Transduction*, 2002, **22**, 431–448.
19 K. Rossbach, S. Wendorff, K. Sander, H. Stark, R. Gutzmer, T. Werfel, M. Kietzmann and W. Baumer, *Exp. Dermatol.*, 2009, **18**, 57–63.
20 R. L. Thurmond, P. J. Desai, P. J. Dunford, W. P. Fung-Leung, C. L. Hofstra, W. Jiang, S. Nguyen, J. P. Riley, S. Sun, K. N. Williams, J. P. Edwards and L. Karlsson, *J. Pharmacol. Exp. Ther.*, 2004, **309**, 404–413.
21 V. Katritch, V. Cherezov and R. C. Stevens, *Trends Pharmacol. Sci.*, 2012, **33**, 17–27.
22 A. J. Kooistra, L. Roumen, R. Leurs, I. J. P. de Esch and C. de Graaf, *Methods Enzymol.*, 2012, in press.
23 T. Shimamura, M. Shiroishi, S. Weyand, H. Tsujimoto, G. Winter, V. Katritch, R. Abagyan, V. Cherezov, W. Liu, G. W. Han, T. Kobayashi, R. C. Stevens and S. Iwata, *Nature*, 2011, **475**, 65–70.
24 C. de Graaf, A. J. Kooistra, H. F. Vischer, V. Katritch, M. Kuijer, M. Shiroishi, S. Iwata, T. Shimamura, R. C. Stevens, I. J. de Esch and R. Leurs, *J. Med. Chem.*, 2011, **54**, 8195–8206.
25 R. Kiss, B. Kiss, A. Konczol, F. Szalai, I. Jelinek, V. Laszlo, B. Noszal, A. Falus and G. M. Keseru, *J. Med. Chem.*, 2008, **51**, 3145–3153.
26 F. Sirci, E. P. Istyastono, H. F. Vischer, A. J. Kooistra, S. Nijmeijer, M. Kuijer, M. Wijtmans, R. Mannhold, R. Leurs, I. J. P. de Esch and C. de Graaf, 2012, Poster presentation: 30th Noorwijkerhout–Camerino–Cyprus Symposium: Trends in Drug Research, http://f1000.com/posters/browse/summary/1090195.
27 Y. Tanrikulu, E. Proschak, T. Werner, T. Geppert, N. Todoroff, A. Klenner, T. Kottke, K. Sander, E. Schneider, R. Seifert, H. Stark, T. Clark and G. Schneider, *ChemMedChem*, 2009, **4**, 820–827.
28 J. S. Surgand, J. Rodrigo, E. Kellenberger and D. Rognan, *Proteins*, 2006, **62**, 509–538.
29 H. Engelhardt, R. A. Smits, R. Leurs, E. Haaksma and I. J. de Esch, *Curr. Opin. Drug Discovery Dev.*, 2009, **12**, 628–643.
30 E. P. Istyastono, C. de Graaf, I. J. de Esch and R. Leurs, *Curr. Top. Med. Chem.*, 2011, **11**, 661–679.
31 R. A. Smits, R. Leurs and I. J. de Esch, *Drug Discovery Today*, 2009, **14**, 745–753.
32 L. Shi and J. A. Javitch, *Annu. Rev. Pharmacol. Toxicol.*, 2002, **42**, 437–467.
33 M. Wijtmans, C. de Graaf, G. de Kloe, E. P. Istyastono, J. Smit, H. Lim, R. Boonnak, S. Nijmeijer, R. A. Smits, A. Jongejan, O. Zuiderveld, I. J. de Esch and R. Leurs, *J. Med. Chem.*, 2011, **54**, 1693–1703.
34 V. Cherezov, D. M. Rosenbaum, M. A. Hanson, S. G. Rasmussen, F. S. Thian, T. S. Kobilka, H. J. Choi, P. Kuhn, W. I. Weis, B. K. Kobilka and R. C. Stevens, *Science*, 2007, **318**, 1258–1265.
35 H. D. Lim, R. M. van Rijn, P. Ling, R. A. Bakker, R. L. Thurmond and R. Leurs, *J. Pharmacol. Exp. Ther.*, 2005, **314**, 1310–1321.
36 H. Engelhardt, I. J. P. de Esch, D. Kuhn, R. A. Smits, O. P. Zuiderveld, J. Dobler, M. Mayer, S. Lips, H. Arnhof, D. Scharn, E. E. J. Haaksma and R. Leurs, *Eur. J. Med. Chem.*, 2012, **54**, 660–668.
37 J. A. Jablonowski, C. A. Grice, W. Chai, C. A. Dvorak, J. D. Venable, A. K. Kwok, K. S. Ly, J. Wei, S. M. Baker, P. J. Desai, W. Jiang, S. J. Wilson, R. L. Thurmond, L. Karlsson, J. P. Edwards, T. W. Lovenberg and N. I. Carruthers, *J. Med. Chem.*, 2003, **46**, 3957–3960.
38 R. Kiss, B. Noszal, A. Racz, A. Falus, D. Eros and G. M. Keseru, *Eur. J. Med. Chem.*, 2008, **43**, 1059–1070.
39 J. D. Venable, H. Cai, W. Chai, C. A. Dvorak, C. A. Grice, J. A. Jablonowski, C. R. Shah, A. K. Kwok, K. S. Ly, B. Pio, J. Wei, P. J. Desai, W. Jiang, S. Nguyen, P. Ling, S. J. Wilson, P. J. Dunford, R. L. Thurmond, T. W. Lovenberg, L. Karlsson, N. I. Carruthers and J. P. Edwards, *J. Med. Chem.*, 2005, **48**, 8289–8298.
40 R. J. Altenbach, R. M. Adair, B. M. Bettencourt, L. A. Black, S. R. Fix-Stenzel, S. M. Gopalakrishnan, G. C. Hsieh, H. Liu, K. C. Marsh, M. J. McPherson, I. Milicic, T. R. Miller, T. A. Vortherms, U. Warrior, J. M. Wetter, N. Wishart, D. G. Witte, P. Honore, T. A. Esbenshade, A. A. Hancock, J. D. Brioni and M. D. Cowart, *J. Med. Chem.*, 2008, **51**, 6571–6580.
41 M. D. Cowart, R. J. Altenbach, H. Liu, G. C. Hsieh, I. Drizin, I. Milicic, T. R. Miller, D. G. Witte, N. Wishart, S. R. Fix-Stenzel, M. J. McPherson, R. M. Adair, J. M. Wetter, B. M. Bettencourt, K. C. Marsh, J. P. Sullivan, P. Honore, T. A. Esbenshade and J. D. Brioni, *J. Med. Chem.*, 2008, **51**, 6547–6557.

42 J. Liu, Y. Li, H. X. Zhang, S. W. Zhang and L. Yang, *J. Mol. Model.*, 2012, **18**, 991–1001.
43 S. P. Meduna, B. M. Savall, H. Cai, J. P. Edwards, R. L. Thurmond and P. M. McGovern, *Bioorg. Med. Chem. Lett.*, 2011, **21**, 3113–3116.
44 C. E. Mowbray, A. S. Bell, N. P. Clarke, M. Collins, R. M. Jones, C. A. Lane, W. L. Liu, S. D. Newman, M. Paradowski, E. J. Schenck, M. D. Selby, N. A. Swain and D. H. Williams, *Bioorg. Med. Chem. Lett.*, 2011, **21**, 6596–6602.
45 K. Sander, T. Kottke, Y. Tanrikulu, E. Proschak, L. Weizel, E. H. Schneider, R. Seifert, G. Schneider and H. Stark, *Bioorg. Med. Chem.*, 2009, **17**, 7186–7196.
46 T. Werner, K. Sander, Y. Tanrikulu, T. Kottke, E. Proschak, H. Stark and G. Schneider, *Chembiochem*, 2010, **11**, 1850–1855.
47 P. H. Keizers, C. de Graaf, F. J. de Kanter, C. Oostenbrink, K. A. Feenstra, J. N. Commandeur and N. P. Vermeulen, *J. Med. Chem.*, 2005, **48**, 6117–6127.
48 A. C. Kruse, J. Hu, A. C. Pan, D. H. Arlow, D. M. Rosenbaum, E. Rosemond, H. F. Green, T. Liu, P. S. Chae, R. O. Dror, D. E. Shaw, W. I. Weis, J. Wess and B. K. Kobilka, *Nature*, 2012, **482**, 552–556.
49 O. Korb, T. Stutzle and T. E. Exner, *J. Chem. Inf. Model.*, 2009, **49**, 84–96.
50 O. Korb, T. Stützle and T. E. Exner, *Lect Notes Comput Sci*, 2006, **4150**, 247–258.
51 E. P. Istyastono. PhD Thesis, 2012.
52 I. Gantz, J. DelValle, L. D. Wang, T. Tashiro, G. Munzert, Y. J. Guo, Y. Konda and T. Yamada, *J. Biol. Chem.*, 1992, **267**, 20840–20843.
53 K. Ohta, H. Hayashi, H. Mizuguchi, H. Kagamiyama, K. Fujimoto and H. Fukui, *Biochem. Biophys. Res. Commun.*, 1994, **203**, 1096–1101.
54 L. Cocco, J. P. Groff, C. Temple, Jr, J. A. Montgomery, R. E. London, N. A. Matwiyoff and R. L. Blakley, *Biochemistry*, 1981, **20**, 3972–3978.
55 P. Czodrowski, I. Dramburg, C. A. Sotriffer and G. Klebe, *Proteins*, 2006, **65**, 424–437.
56 G. J. Sterk, H. van der Goot and H. Timmerman, *Eur. J. Med. Chem.*, 1984, **19**, 545.
57 H. D. Lim, R. A. Smits, R. A. Bakker, C. M. van Dam, I. J. de Esch and R. Leurs, *J. Med. Chem.*, 2006, **49**, 6650–6651.
58 B. Lenarcik and M. Wisniewski, *Polish. J. Chem*, 1983, **57**, 735–744.
59 P. R. Reddy, N. Raju, K. S. Rao and A. Shilpa, *Indian J. Chem.*, 2009, **48**, 761–768.
60 T. Vitali, M. Impicciatore, C. Ferrari and G. Morini, *Farmaco, Ed. Sci.*, 1980, **35**, 366–379.
61 I. Kufareva, M. Rueda, V. Katritch, Participants, G. D., R. C. Stevens and R. Abagyan, *Structure*, 2011, **19**, 1108–1126.
62 M. Michino, E. Abola, Participants, G. D., C. L. Brooks, III, J. S. Dixon, J. Moult and R. C. Stevens, *Nat. Rev. Drug Discovery*, 2009, **8**, 455–463.
63 C. de Graaf and D. Rognan, *Curr. Pharm. Des.*, 2009, **15**, 4026–4048.
64 D. A. Goldfeld, K. Zhu, T. Beuming and R. A. Friesner, *Proc Natl Acad Sci USA*, 2011, **108**, 8275–8280.
65 C. de Graaf, N. Foata, O. Engkvist and D. Rognan, *Proteins*, 2008, **71**, 599–620.
66 E. Stjernschantz and C. Oostenbrink, *Biophys. J.*, 2010, **98**, 2682–2691.
67 M. Bruysters, A. Jongejan, A. Akdemir, R. A. Bakker and R. Leurs, *J. Biol. Chem.*, 2005, **280**, 34741–34746.
68 A. Heifetz, G. B. Morris, P. C. Biggin, O. Barker, T. Fryatt, J. Bentley, D. Hallett, D. Manikowski, S. Pal, R. Reifegerste, M. Slack and R. Law, *Biochemistry*, 2012, **51**, 3178–3197.
69 R. I. Allen, K. J. Box, J. E. Comer, C. Peake and K. Y. Tam, *J. Pharm. Biomed. Anal.*, 1998, **17**, 699–712.
70 G. Volgyi, R. Ruiz, K. Box, J. Comer, E. Bosch and K. Takacs-Novak, *Anal. Chim. Acta*, 2007, **583**, 418–428.
71 Chemical Computing Group (CCG) MOE (Molecular Operating Environment) v.2009.10, Montreal, 2009, http://www.chemcomp.com/software.htm.
72 D. A. Case, T. A. Darden, T. E. Chatman III, C. W. J. Simmerling, R. E. Duke, R. Luo, M. Crowley, R. C. Walker, W. Zhang, K. M. Merz, B. Wang, S. Hayik, A. Roitberg, G. Seabra, I. Kolossvary, K. F. Wong, F. Paesani, J. Vanicek, X. Wu, S. R. Brozell, T. Steinbrecher, H. Gohlke, L. Yang, C. Tan, J. Mongan, V. Hornak, G. Cui, D. H. Mathews, M. G. Seetin, C. Sagui, V. Babin and P. A. Kollman, *AMBER10*, 2008.
73 E. Urizar, S. Claeysen, X. Deupi, C. Govaerts, S. Costagliola, G. Vassart and L. Pardo, *J. Biol. Chem.*, 2005, **280**, 17135–17141.
74 H. J. C. Berendsen, J. P. M. Postma, W. F. van Gunsteren, A. DiNola and J. R. Haak, *J. Chem. Phys.*, 1984, **81**, 3684–3690.
75 Y. Duan, C. Wu, S. Chowdhury, M. C. Lee, G. Xiong, W. Zhang, R. Yang, P. Cieplak, R. Luo, T. Lee, J. Caldwell, J. Wang and P. Kollman, *J. Comput. Chem.*, 2003, **24**, 1999–2012.
76 J. Wang, R. M. Wolf, J. W. Caldwell, P. A. Kollman and D. A. Case, *J. Comput. Chem.*, 2004, **25**, 1157–1174.
77 J. Wang, W. Wang, P. A. Kollman and D. A. Case, *J. Mol. Graphics Modell.*, 2006, **25**, 247–260.
78 G. Marcou and D. Rognan, *J. Chem. Inf. Model.*, 2007, **47**, 195–207.
79 J. D. Durrant, C. A. de Oliveira and J. A. McCammon, *J. Mol. Graphics Modell.*, 2011, **29**, 773–776.

